# Colloidal Metal−Organic Framework Hexapods Prepared from Postsynthesis Etching with Enhanced Catalytic Activity and Rollable Packing

Zihao Ou,[†,‡] Xiaohui Song,[†,‡] Wen Huang,[§,‖] Xing Jiang,[⊥] Subing Qu,[‡] Qingyi Wang,[§] Paul V. Braun,[‡,#,△] Jeffrey S. Moore,[⊥,△] Xiuling Li,[§,#] and Qian Chen*[,‡,⊥,#,△]

‡Department of Materials Science and Engineering, §Department of Electrical and Computer Engineering, Micro and Nanotechnology Laboratory, ⊥Department of Chemistry, #Frederick Seitz Materials Research Laboratory, and △Beckman Institute for Advanced Science and Technology, University of Illinois, Urbana, Illinois 61801, United States

S *Supporting Information*
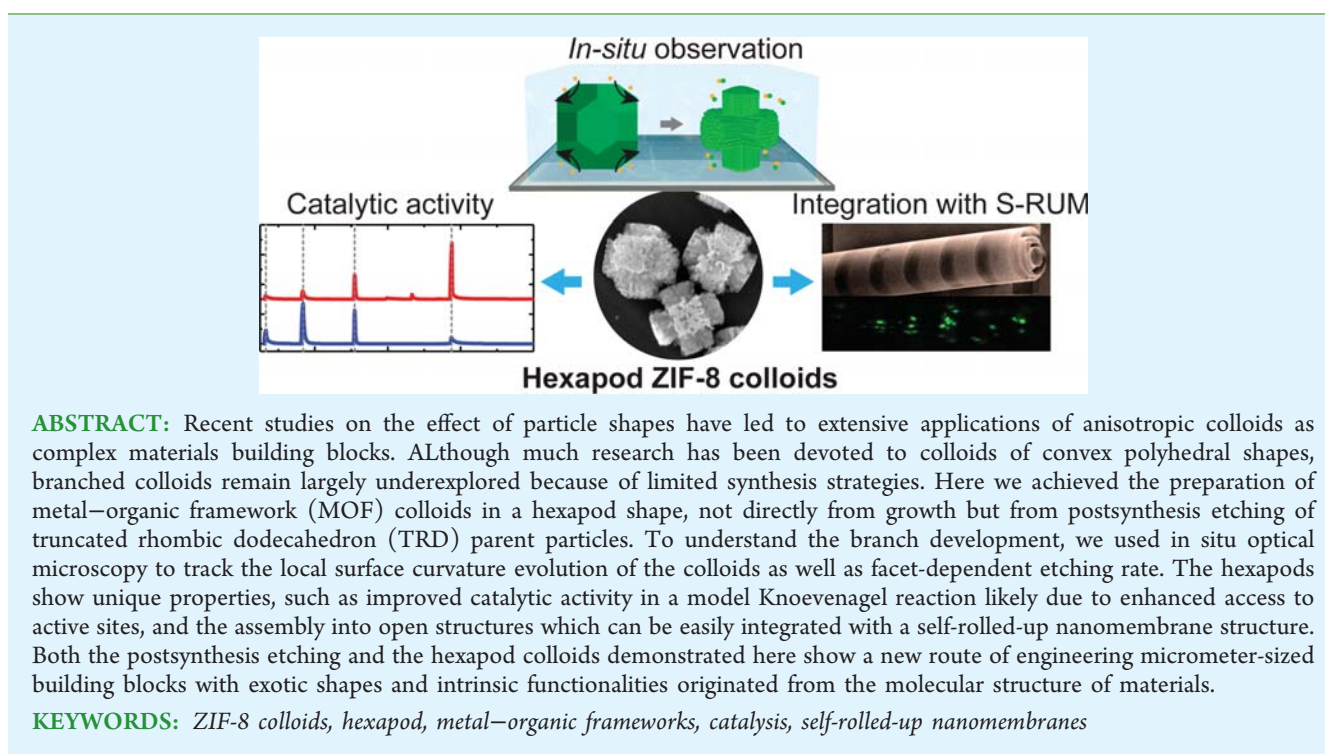
ABSTRACT: Recent studies on the effect of particle shapes have led to extensive applications of anisotropic colloids as complex materials building blocks. ALthough much research has been devoted to colloids of convex polyhedral shapes, branched colloids remain largely underexplored because of limited synthesis strategies. Here we achieved the preparation of metal−organic framework (MOF) colloids in a hexapod shape, not directly from growth but from postsynthesis etching of truncated rhombic dodecahedron (TRD) parent particles. To understand the branch development, we used in situ optical microscopy to track the local surface curvature evolution of the colloids as well as facet-dependent etching rate. The hexapods show unique properties, such as improved catalytic activity in a model Knoevenagel reaction likely due to enhanced access to active sites, and the assembly into open structures which can be easily integrated with a self-rolled-up nanomembrane structure. Both the postsynthesis etching and the hexapod colloids demonstrated here show a new route of engineering micrometer-sized building blocks with exotic shapes and intrinsic functionalities originated from the molecular structure of materials.

KEYWORDS: *ZIF-8 colloids, hexapod, metal−organic frameworks, catalysis, self-rolled-up nanomembranes*

Anisotropic colloids have been extensively studied as structural and functional building blocks for complex materials.[1] Compared with convex polyhedron shapes (cube, rods, octahedron, tetrahedron, etc.), for which a line connecting any two (noncoplanar) points on the surface lies in the interior of the polyhedron,[2] branched colloids are gaining increasing importance for various applications unique to their geometry.[3−5] For example, achiral planar colloidal "crosses" have been shown to assemble into symmetry breaking chiral structures due to the branch interlocking between crosses.[6] Nanosized CdSe/CdS tetrapods have been used as stress sensors with fluorescence emission responsive to branch bending caused by local tensile/compressive stress.[7] Sharp tips of gold nanostars are known to locally concentrate electromagnetic field and achieve exceptional surface enhanced Raman resonance.[8] In these and other examples, the branch morphology introduces self-assembly and properties not readily accessible to convex polyhedral. However, studies on branched colloids remain largely underexplored because of limited synthesis methods and particle composition. Generation of branches involves creating additional surface area in an anisotropic way and producing surfaces of negative curvature, which is often thermodynamically unfavored. On the nanoscale, it has been mainly realized in metallic and semiconducting nanoparticles by directional growth upon preformed faceted crystalline seeds in abundant passivating ligands.[3−5] On the micrometer-scale, photolithography has been used instead to pattern branches,[6] which is limited to

A

49 photoresist materials such as SU-8, two-dimensional (2D)
50 colloidal shapes and hard to scale up. Recent pioneering work
51 demonstrated the synthesis of micron-sized silica hexapods by
52 utilizing faceted seeds.[9] Yet synthesis of branched colloids of
53 other functional composition is currently lacking.

54   Here we achieved the preparation of metal−organic
55 framework (MOF) colloids with a hexapod shape, not directly
56 from growth but from postsynthesis etching of parent particles
57 of a convex polyhedron shape. The branch development from
58 truncated rhombic dodecahedron (TRD) to the final hexapod
59 shape was tracked in real-time under optical microscopy, which
60 elucidates the facet-dependent etching rate as a crucial reason
61 for the shape transformation. Here the MOF colloids are
62 composed of ZIF-8, where Zn^{2+} ions are connected by 2-
63 methylimidazole (2-MIM) linkers into a three-dimensional
64 (3D) microporous architecture useful for catalysis, filtration,
65 and gas storage applications.[10,11] The etching occurs via acid−
66 base reactions demonstrated in an earlier work, where Zn^{2+}
67 ions are sequestered and chelated by xylenol orange (XO) as
68 the etchant.[12] The partial removal of metal ions or ligands
69 from the microporous MOF structure not only leads to a shape
70 change in the colloids, but also generates nanostructured
71 roughness while maintaining in part the original microporosity.
72 As a result, when applied to a model Knoevenagel reaction, the
73 hexapod ZIF-8 colloids have 9-fold increase in catalytic activity
74 than the parent TRD colloids of the same weight. In addition,
75 the hexapod shape renders the colloids geometrically intriguing
76 as they do not assemble into space-filling lattices when packed
77 in 2D. The interstitial space thus makes the 2D colloidal layer
78 compatible with flexible substrates. In our proof-of-concept
79 experiment, the hexapod ZIF-8 colloids are loaded as a 2D
80 layer onto a self-rolled-up nanomembrane (S-RUM) platform,
81 a recent advancement we developed to roll an otherwise flat,
82 microfabricated substrate into a tubular structure. Upon the
83 membrane rolling-up, the 2D layer of colloidal hexapods
84 accommodates the closer packing, which can potentially lead
85 to reconfigurable hybrid material comprising colloids and
86 fabricated device membranes.

87   The hexapod ZIF-8 colloids were prepared via a two-step
88 process (Figure 1 and the Supporting Information). First, we
89 followed a literature method[13] to synthesize monodisperse
90 TRD-shaped ZIF-8 colloids as the parent colloids. This
91 method involves the use of dual capping ligands of 1-
92 methylimidazole (1-MIM) and poly(vinylpyrrolidone) (PVP,
93 Mw ∼360 000), whose concentration is used to fine-tune the
94 particle dimension. As shown in Figure 1A, the TRD ZIF-8
95 parent colloids contain 6 square {100} facets and 12 hexagonal
96 {110} facets, effectively a rhombic dodecahedron with
97 truncation at 6 corners.[12,14] Two parameters were used to
98 describe the particle size: L for the overall particle size and x
99 for the truncation (side length of the square facet). The
100 corresponding truncation ratio m is defined as x/L, which
101 ranges from 0.15 to 0.39 in different batches. The parent
102 colloids obtained in this method are of a high monodispersity
103 (Figure S1, Table 1). Second, we adopted the XO etchant
104 solution for ZIF-8 reported by Avci et al. in our TRD
105 colloids.[12] In their work, convex polygonal shapes were
106 produced after etching, whereas our work obtained branched
107 hexapods instead, likely due to the differences in the parent
108 particle synthesis (e.g., capping ligands, particle sizes, solvent).
109 Beyond the demonstrated usage for ZIF-8 colloidal etching,
110 this XO etchant solution was chosen for our study because it
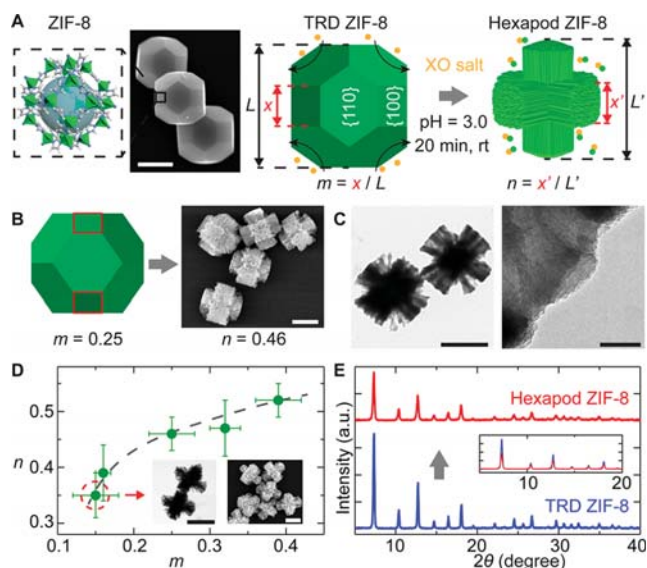111 has two independent molecular aspects to facilitate the precise

Figure 1. Hexapod ZIF-8 colloids prepared via postsynthesis etching. (A) Left: Scanning electron microscopy (SEM) image of the TRD ZIF-8 parent colloids and a zoomed-in schematic showing the ZIF-8 molecular structure. Right: Schematics showing that etching produces the hexapod ZIF-8 colloids from the TRD ZIF-8 parent colloids, with the shape parameters labeled. (B) Schematics of the TRD ZIF-8 parent colloids and a SEM image of the hexapod ZIF-8 colloids rendered from etching. (C) Transmission electron microscopy (TEM) images of the hexapod ZIF-8 colloids in (B). (D) A graph relating the truncation ratio m of the TRD ZIF-8 parent colloids to the branching ratio n of the final hexapod colloids. Inset: TEM and SEM images of hexapod colloids ($n = 0.35$) etched from TRD ZIF-8 parent colloids ($m = 0.15$). (E) X-ray diffraction (XRD) spectra of the TRD ZIF-8 parent colloids (blue, $m = 0.37$) and the hexapod ZIF-8 colloids (red, $n = 0.35$). Inset: XRD spectra from 5 to 20° are presented without shifting. Scale bars: SEM images in A−D, zoomed-out TEM image in C, 2 μm; zoomed-in TEM image in C, 100 nm.

control of etching kinetics.[15,16] For one, the XO etchant 112
solution is acidic, which protonates 2-MIM in the MOF 113
colloids and breaks the connection between Zn^{2+} and 2-MIM 114
linkers. For the other, XO acts as a chelating agent that 115
coordinates with the liberated Zn^{2+} ions to form into water- 116
soluble complex, thereby further favoring the etching. In a 117
typical experiment of ours, a solution of TRD ZIF-8 colloids 118
(500 μL, 10−16 mg/mL in ethanol) was mixed with a XO 119
etchant solution (500 μL, pH = 3.0, 16 mg/mL) under 120
constant stirring at 500 rpm for 20 min. Monodisperse 121
hexapod ZIF-8 colloids with 6 protruding branches were 122
obtained after etching as shown in Figure 1B−C and Figure S1. 123
Their solution-phase self-assembly (Figure S3) observed under 124
optical microscopy shows the formation of interlocked chains, 125
consistent with the branched nanoparticles reported earlier.[3] 126
Similar to the truncation ratio m for the TRD parent colloids, a 127
branching ratio $n = x'/L'$ is employed to characterize the shape 128
of the hexapod particles, where L' is for the overall size of the 129
hexapods and x' for the branch width (Table 1). 130

   The hexapod ZIF-8 colloids exhibit porous surface features 131
after etching, their branching ratio related one-to-one with the 132
truncation ratio of parent colloids. The SEM and TEM images 133
of the hexapod colloids show grooves and pores of 80−200 nm 134
in size (Figure 1B, C), whereas smooth surfaces were observed 135
in the parent colloids before etching (Figure 1A and Figure 136
S1). This observation is likely due to the working mechanism 137

Table 1. Size and Shape Characterization of the TRD ZIF-8 Parent Colloids and the Corresponding Hexapod ZIF-8 Colloids Given in Figure S1[a]

TRD ZIF-8 parent colloids			Hexapod ZIF-8 colloids		
L (μm)	x (μm)	$m = x/l$	L' (μm)	x' (μm)	$n = x'/L'$
3.73 ± 0.22	0.54 ± 0.11	0.15 ± 0.03	3.30 ± 0.22	1.14 ± 0.11	0.35 ± 0.04
1.98 ± 0.04	0.31 ± 0.03	0.16 ± 0.01	1.52 ± 0.08	0.59 ± 0.06	0.39 ± 0.05
4.22 ± 0.16	1.05 ± 0.10	0.25 ± 0.03	3.03 ± 0.14	1.39 ± 0.12	0.46 ± 0.03
2.33 ± 0.11	0.75 ± 0.05	0.32 ± 0.02	2.18 ± 0.08	1.02 ± 0.10	0.47 ± 0.05
2.73 ± 0.26	1.05 ± 0.09	0.39 ± 0.03	2.50 ± 0.21	1.28 ± 0.07	0.52 ± 0.03

[a]The shape parameters L, x, L', and x' were measured directly from SEM images.

of the etchant: both Zn^{2+} and 2-MIM linkers constituting the MOF are expected to be leached out[12] and induce destruction or roughening of the MOF particle surface. The branching ratio of the hexapods hinges on the truncation ratio of the parent colloids, because the branches are developed from the square faces of a 6-fold symmetry in the TRD shapes. Under the same etching condition, the TRD parent colloids of a smaller truncation ratio produce hexapods of a smaller branching ratio, as demonstrated in the m–n curve from multiple synthesis (Figure 1D, Figure S1 and S2). Despite the shape change, the hexapod ZIF-8 colloids retained the original microporous MOF structure as suggested by the XRD (Figure 1E). Although the intensity is reduced for the hexapod ZIF-8 colloids given the same sample weight, and the full widths at half-maximum of peaks are larger than the TRD parent colloids, the XRD patterns exhibit only peaks ascribed to ZIF-8, confirming the maintenance of crystallinity.

To elucidate how the hexapod branches are developed from convex polygonal parent particles, we imaged and tracked the etching of ZIF-8 colloids in situ under optical microscopy. The positively charged TRD ZIF-8 parent colloids[13] (when dispersed in ethanol) were attached to the negatively charged glass substrate during the imaging, which minimizes the disturbance from the solvent flow while adding aliquots of the etchant solution (Figure 2A). Multiple particles attached in different orientations were recorded during the etching process, which follow the same type of etching trajectory as shown in Figure S4. In our quantitative analysis, a particle with one {110} facet on the substrate was selected because it is the most probable sitting orientation of parent particles (~79%, see Figures S1 and S4). Automatic image processing was applied to the captured optical microscopy movies, generating binarized frames and outlining the contours of the particle projections (Figures 2B and Figures S5). The local curvature along the contours was determined,[17,18] facilitating parametrization of branch developments during the shape transformation (Figure 2C, Movie S1).

The temporal evolution of particle contours reveals a facet-dependent etching rate responsible for the branch formation. Figure 2D overlays contours spanning over the whole etching process (~300 s) with the contour centers corrected to overlap. For the first 90 s, the contours shrink slightly in a uniform manner and the TRD shape was maintained. Yet after this time, the {110} hexagonal facets became unstable and etched faster than the {100} square facets. This uneven etching rate gives rise to the concave (i.e., negative curvature) regions colored in blue, which grows into the final cross shape. Then the particle shape contour stabilizes which suggests the reaction has reached equilibrium. The branching was further quantified by the local curvature distributions of the contour series. As shown in Figure 2E, the starting distribution contains
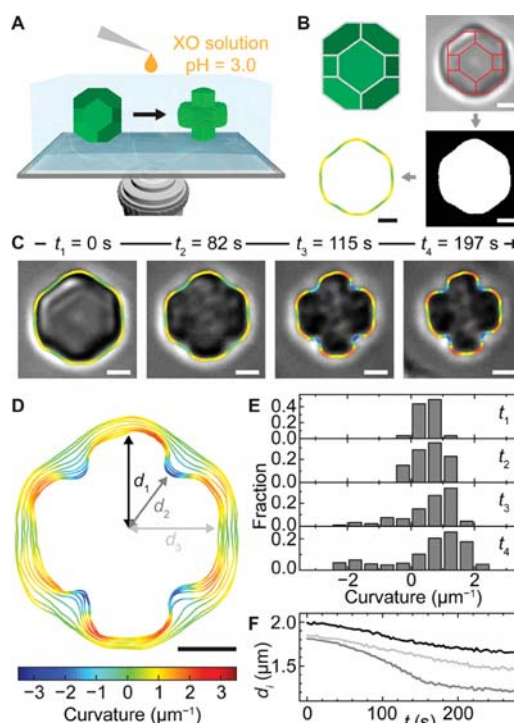

Figure 2. Direct imaging of etching dynamics from the parent TRD to hexapod ZIF-8 colloids. (A) Schematic of optical microscopy experimental setup. (B) Automatic contour detection for imaged particles. Top: schematic and optical microscopy image (overlaid with schematic) of a TRD ZIF-8 particle with {110} facing the substrate. Bottom: contour detection achieved by binarizing the image and tracing the black-white boundary. (C) Time-lapse optical microscopy images of the same particle during etching with tracked contours overlaid. (D) Time-lapse shape contours (10 contours in total, 29 s interval) showing the branching process. (E) Distributions of local curvatures calculated from four contours selected from C. (F) Temporal evolution of the distances d_1 (black), d_2 (gray), and d_3 (light gray) following directions labeled in D. All contours in B–D are colored according to the local curvatures following the color map in D. Scale bars: 1 μm.

only a single peak and positive curvatures, which is characteristic of TRD, which later broadens into a bimodal distribution covering both positive and negative curvatures, indicating the branch formation. The facet-dependence of the etching rate was further characterized by measuring the center-to-edge distance d_i along three different directions. At first, all distances decreased at similar rates (slopes), while after 90 s, d_2 decreases drastically with a slope larger than those of d_1 and d_3 until all three curves flattened. Movie S1 shows a synchronized shape evolution of the selected particle with the curvature
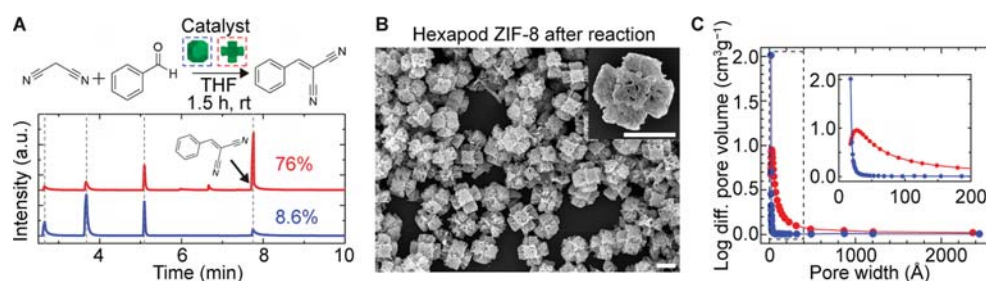
Figure 3. Catalytic activity of hexapod and TRD ZIF-8 colloids. (A) Model Knoevenagel reaction (top) and GC−MS traces (bottom) of the reaction mixtures after 1.5 h using hexapod (red) and TRD (blue) ZIF-8 colloids as the catalysts. The dotted lines in the traces denote, from left to right, peaks corresponding to malononitrile, benzaldehyde, 1,2,4,5-tetramethylbenzene (internal standard)m and benzylidenemalononitrile. (B) Large-view SEM image of the hexapod ZIF-8 colloids after reaction. Inset is a zoomed-in view. Scale bars: 2 μm. (C) Log differential pore distribution profiles of the hexapod (red) and TRD (blue) ZIF-8 colloids. Inset is a magnified view of the boxed region.

distribution and three center-to-edge distances to highlight the etching dynamics. Such facet-dependent etching rate is probably due to different capping ligand densities on the TRD ZIF-8 parent colloid facets, which passivate distinctly the surface ions and linkers.[13] XO molecules are bulky in size, capable only of diffusing into surface pores of the colloids to achieve etching. As a result, the final hexapod colloids maintain the ZIF-8 crystallinity (Figure 1E), not undergoing a complete destruction. The strong bond between Zn^{2+} and 2-MIM linkers, as well as the passivation from abundant capping ligands hold the shape rendered by XO etchant intact against postetching restructuring. Such delicate interplay between facet-dependent ligand binding and molecular reactions can be potentially modulated with ligand choice in synthesis. Direct visualization of the shape transformation trajectories can also offer the opportunity to design MOF colloids over a large shape space and provides fundamental insights into the nonequilibrium growth/etching mechanism of crystals.[18,19]

Now that we understand hexapod formation, we study how the etching-rendered hexapod geometry impacts the catalytic activity of colloidal ZIF-8. ZIF-8 MOF has been demonstrated as great heterogeneous catalysts due to the abundant Lewis acid sites from Zn^{2+} and basic sites from N-moieties.[20−22] A recent study suggests that only the external surface of ZIF-8 is catalytically active, not the microporous structure imbedded inside the bulk crystal.[23] To evaluate the effect of shapes, we used both the TRD ZIF-8 and hexapod ZIF-8 colloids as catalysts in the model Knoevenagel reaction between benzaldehydes and malononitriles (Figure 3A). The hexapod ZIF-8 colloids exhibit a 9-fold increase in the catalytic activities with respect to the TRD ZIF-8 colloids. As shown in Figure 3A, the benzaldehyde conversions, 76% for the hexapods and 8.6% for the TRD colloids, were measured from gas chromatography− mass spectroscopy (GC−MS) of the reaction mixture 1.5 h after the reaction at room temperature, with 1,2,4,5-tetramethylbenzene as an internal standard. SEM of the hexapod colloids shows no obvious altering of the shape (Figure 3B). This increase in the catalytic activity, despite the same MOF structure (Figure 1E), can be attributed by the larger apparent surface area-to-volume ratio in the hexapods than TRD colloids, which facilitates the accessibility of reactive sites.[24] In contrast, the micropores in the TRD colloids largely reside in the bulk matrix and result in lower diffusion efficiency and less accessibility to bulky reactants. Moreover, the pore-size distribution profile of the hexapod colloids, calculated from the N_2 adsorption isotherm (Figure S6) by the Barrett−Joyner−Halenda (BJH) method, shows a peak at 26 Å on the

log differential pore volume profile, not seen in the TRD colloids, as well as a tail in the larger pore size side (Figure 3C). These large pores are not expected for the conventional ZIF-8 crystal whose intrinsic pore width is 11.6 Å.[25] Their presence in the hexapod colloids can be attributed to partial removal of metal ions and/or linkers from the original MOF. Note that similar change in pore size distribution has been observed in the postsynthesis processing of other MOFs like selective acid etching of MIL-100(Fe)[26] and hydrolytic transformation of POST-66(Y),[27] where the larger pore size can allow the reactants to diffuse faster compared within a bulky MOF crystal.[28] Regarding cyclability of ZIF-8 colloids as catalyst, previous work[28] shows that they can be used for seven times with high performance maintained, without obvious blocking of accessible pores.

Lastly, in the context of colloidal self-assembly, the hexapod ZIF-8 colloids pack less densely in 2D due to the branch geometry than the TRD ones when both are concentrated. As shown in Figure 4A, the hexapods partially interlock and exhibit interstitial space allowing local rearrangement, while the TRD colloids pack closely into a hexagonal lattice. Here we chose hexapods of a large branching ratio ($n = 0.35$) as they form into interlocked structures more easily (Figure S1), consistent with recent simulation studies on branched nanocrystals.[29] This packing introduces an intriguing opportunity to integrate the hexapods with actuating substrates, such as the self-rolled-up nanomembrane (S-RUM) platform developed earlier by us.[30−32] The S-RUM platform was prepared following a literature method,[30] with layered structures shown in Figure S7, where the square wave like patterned 5 nm thick Nickle strip has tensile stress embedded to enhance the rolling force to overcome a heavy rolling load. By opening a window on one side of the mesa, the Ge sacrificial layer can be continuously removed by an etchant solution to trigger the rolling. When we deposited a 2D layer of hexapod colloids dispersed in dimethylformamide (DMF) onto the S-RUM platform by drop casting (Figure 4B and the Supporting Information), the self-rolling was successful as captured by optical microscopy (Figure 4C). The incorporation of the hexapods into the final tubular structures was also verified both by SEM (Figure 4D) and fluorescence optical microscopy imaging (Figure 4E, Movie S2) as the organic linker in ZIF-8 (2-MIM) has intrinsic fluorescence.[33] SEM images of the S-RUM loaded with hexapods show an interlayer spacing between the adjacent rolled layers, where the hexapods sitting in between acted like a spacer. In comparison, the S-RUM without colloids loaded has adjacent layers in physical
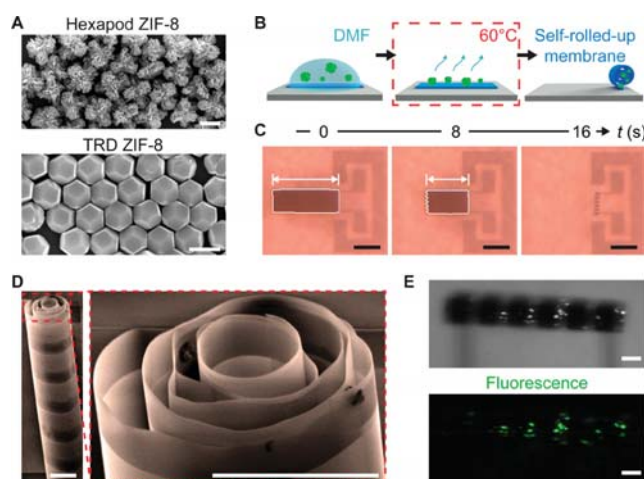
Figure 4. Rolling of the S-RUM platform loaded with the hexapod ZIF-8 colloids. (A) SEM images of the hexapod (top) and the TRD (bottom) ZIF-8 colloidal monolayers. (B) Schematics showing the loading of hexapods onto S-RUM and its rolling-up: hexapod solution in DMF was first drop cast onto the substrate, which was heated at 60 °C for 2 h to fully dry. By etching the sacrificial Ge layer (Figure S7), self-rolling can be achieved with hexapods loaded inside. (C) Time-lapse optical microscopy images of the rolling-up process, with the unrolled part of the substrate tracked by the white contour. (D) Pseudocolored SEM images of the S-RUM with hexapods loaded. (E) Optical microscopy images of a S-RUM loaded with hexapods under white light and laser (top), and laser only (bottom). Scale bars: (A) 2 μm, (C) 200 μm, (D, E) 20 μm.

contact (Figure S8B). In our control experiment of the S-RUM loaded with TRD colloids, the self-rolling was not successful (Figure S8C). We see that the nonconvex shapes of hexapods can accommodate more interlocking as the S-RUM substrate becomes curved and reduce the resistance against the rolling-up. This integration can thus be potentially used to study colloidal self-assembly on curved 3D surface,[34] modulate the structures of S-RUM platform as well as realize multifunctional devices incorporating the functions of the MOF colloids, such as responsive refractive index via loading gas molecules into the molecular pores of MOF crystals.[14]

In summary, we presented an experimental preparation of hexapod ZIF-8 colloids via postsynthesis etching methods. We elucidate that the branch formation was induced by facet-dependent etching as monitored by real-time optical microscopy imaging of the etching process. The hexapods show a 9-fold increase in catalytic activity due to the greatly enhanced accessible catalytic sites. The branch geometry also renders low density packing structures with enough interstitial space to accommodate a curved substrate using our S-RUM system as a demonstration. We foresee the hexapods and the postsynthesis etching method enrich the shape and material library of colloids with improved functions, such as catalytic activities and photoluminescence, and potential applications in the microfabrication design of reconfigurable and multifunctional devices. Our mechanistic and application study suggests opportunities in using other etchant candidates and other types of MOF colloids. For example, gallic acid was shown to etch ZIF-8 MOF upon protonation of 2-MIM linkers,[35] while ethylenediaminetetraacetic acid chelates with Zn^{2+} strongly and can potentially work as ZIF-8 MOF etchant at low pH.[36] MOF containing other ions, such as ZIF-67 (Co^{2+}) with similar facet stability to that of ZIF-8,[12] can potentially adopt similarly unconventional geometry with extensive optimization of facet-dependent etching rates.

ASSOCIATED CONTENT

Ⓢ Supporting Information

The Supporting Information is available free of charge on the ACS Publications website at DOI: 10.1021/acsami.8b17477.

> Chemicals; synthesis details of the TRD ZIF-8 parent colloids and hexapod ZIF-8 colloids; SEM/TEM of TRD and hexapod ZIF-8 colloids; bright-field and fluorescence microscopy imaging, XRD, pore size distribution, zeta potential measurement of the ZIF-8 colloids; catalytic activity measurements; contour identification for mapping the shape transformation during etching; fabrication details of S-RUM; preparation of particle monolayer on S-RUM (PDF)
>
> Movie S1, single particle etching trajectory(AVI)
>
> Movie S2, confocal scanning over a S-RUM loaded with hexapod ZIF-8 colloids (AVI)

AUTHOR INFORMATION

Corresponding Author
*Email: qchen20@illinois.edu.

ORCID
Paul V. Braun: 0000-0003-4079-8160
Qian Chen: 0000-0002-1968-441X

Present Address
‖W.H. is currently at School of Electronic Science and Applied Physics, Hefei University of Technology, Hefei 230009, PR China.

Author Contributions
†Z. O. and X. S. contributed equally. The manuscript was written through contributions of all authors. All authors have given approval to the final version of the manuscript.

Notes
The authors declare no competing financial interest.

ABBREVIATIONS

MOF, metal−organic framework; TRD, truncated rhombic dodecahedron; S-RUM, self-rolled-up membrane; XO, xylenol orange; 1-MIM, 1-methylimidazole; 2-MIM, 2-methylimidazole; PVP, poly(vinylpyrrolidone);; SEM, scanning electron microscopy; TEM, transmission electron microscopy; XRD, X-ray diffraction.

■ REFERENCES

(1) Damasceno, P. F.; Engel, M.; Glotzer, S. C. Predictive Self-Assembly of Polyhedra into Complex Structures. *Science* **2012**, *337* (6093), 453−457.

(2) Duijvestijn, A.; Federico, P. The Number of Polyhedral (3-Connected Planar) Graphs. *Math. Comp.* **1981**, *37* (156), 523−532.

(3) Miszta, K.; de Graaf, J.; Bertoni, G.; Dorfs, D.; Brescia, R.; Marras, S.; Ceseracciu, L.; Cingolani, R.; van Roij, R.; Dijkstra, M.; Manna, L. Hierarchical Self-Assembly of Suspended Branched Colloidal Nanocrystals into Superlattice Structures. *Nat. Mater.* **2011**, *10*, 872.

(4) Li, H.; Kanaras, A. G.; Manna, L. Colloidal Branched Semiconductor Nanocrystals: State of the Art and Perspectives. *Acc. Chem. Res.* **2013**, *46* (7), 1387−1396.

(5) Ye, E. Y.; Regulacio, M. D.; Zhang, S. Y.; Loh, X. J.; Han, M. Y. Anisotropically Branched Metal Nanostructures. *Chem. Soc. Rev.* **2015**, *44* (17), 6001−6017.

(6) Zhao, K.; Mason, T. G. Self-Organized Chiral Colloidal Crystals of Brownian Square Crosses. *J. Phys.: Condens. Matter* **2014**, *26* (15), 152101.

(7) Raja, S. N.; Zherebetskyy, D.; Wu, S.; Ercius, P.; Powers, A.; Olson, A. C. K.; Du, D. X.; Lin, L.; Govindjee, S.; Wang, L.-W.; Xu, T.; Alivisatos, A. P.; Ritchie, R. O. Mechanisms of Local Stress Sensing in Multifunctional Polymer Films Using Fluorescent Tetrapod Nanocrystals. *Nano Lett.* **2016**, *16* (8), 5060−5067.

(8) Khoury, C. G.; Vo-Dinh, T. Gold Nanostars For Surface-Enhanced Raman Scattering: Synthesis, Characterization and Optimization. *J. Phys. Chem. C* **2008**, *112* (48), 18849−18859.

(9) Kim, J.-H.; Hwang, H. J.; Oh, J. S.; Sacanna, S.; Yi, G.-R. Monodisperse Magnetic Silica Hexapods. *J. Am. Chem. Soc.* **2018**, *140* (29), 9230−9235.

(10) Jiao, L.; Wang, Y.; Jiang, H.-L.; Xu, Q. Metal−Organic Frameworks as Platforms for Catalytic Applications. *Adv. Mater.* **2018**, *30* (37), 1703663.

(11) Kirchon, A.; Feng, L.; Drake, H. F.; Joseph, E. A.; Zhou, H.-C. From Fundamentals to Applications: A Toolbox for Robust and Multifunctional MOF Materials. *Chem. Soc. Rev.* **2018**, DOI: 10.1039/C8CS00688A,

(12) Avci, C.; Ariñez-Soriano, J.; Carné-Sánchez, A.; Guillerm, V.; Carbonell, C.; Imaz, I.; Maspoch, D. Post-Synthetic Anisotropic Wet-Chemical Etching of Colloidal Sodalite ZIF Crystals. *Angew. Chem., Int. Ed.* **2015**, *54* (48), 14417−14421.

(13) Yanai, N.; Sindoro, M.; Yan, J.; Granick, S. Electric Field-Induced Assembly of Monodisperse Polyhedral Metal-Organic Framework Crystals. *J. Am. Chem. Soc.* **2013**, *135* (1), 34−37.

(14) Avci, C.; Imaz, I.; Carné-Sánchez, A.; Pariente, J. A.; Tasios, N.; Pérez-Carvajal, J.; Alonso, M. I.; Blanco, A.; Dijkstra, M.; López, C.; Maspoch, D. Self-Assembly of Polyhedral Metal-Organic Framework Particles into Three-Dimensional Ordered Superstructures. *Nat. Chem.* **2017**, *10*, 78−84.

(15) Študlar, K.; Janoušek, I. The Photometric Determination of Zinc with Xylenol Orange. *Talanta* **1961**, *8* (4), 203−208.

(16) Ogura, K.; Kurakami, S.; Seneo, K. Electroanalytical and Spectroscopic Studies on Metal Complexes with Sulphonephthalein Derivatives—II: Fe(III), Co(II), Ni(II), Cu(II) and Zn(II) Complexes with Xylenol Orange. *J. Inorg. Nucl. Chem.* **1981**, *43* (6), 1243−1247.

(17) Kim, J.; Ou, Z.; Jones, M. R.; Song, X.; Chen, Q. Imaging the Polymerization of Multivalent Nanoparticles in Solution. *Nat. Commun.* **2017**, *8* (1), 761.

(18) Ye, X.; Jones, M. R.; Frechette, L. B.; Chen, Q.; Powers, A. S.; Ercius, P.; Dunn, G.; Rotskoff, G. M.; Nguyen, S. C.; Adiga, V. P.; Zettl, A.; Rabani, E.; Geissler, P. L.; Alivisatos, A. P. Single-Particle Mapping of Nonequilibrium Nanocrystal Transformations. *Science* **2016**, *354* (6314), 874−877.

(19) Patterson, J. P.; Abellan, P.; Denny, M. S.; Park, C.; Browning, N. D.; Cohen, S. M.; Evans, J. E.; Gianneschi, N. C. Observing the Growth of Metal-Organic Frameworks by in Situ Liquid Cell Transmission Electron Microscopy. *J. Am. Chem. Soc.* **2015**, *137* (23), 7322−7328.

(20) Guan, Y.; Shi, J.; Xia, M.; Zhang, J.; Pang, Z.; Marchetti, A.; Wang, X.; Cai, J.; Kong, X. Monodispersed ZIF-8 Particles with Enhanced Performance for CO2 Adsorption and Heterogeneous Catalysis. *Appl. Surf. Sci.* **2017**, *423*, 349−353.

(21) Yang, Q.; Xu, Q.; Yu, S.-H.; Jiang, H.-L. Pd Nanocubes@ZIF-8: Integration of Plasmon-Driven Photothermal Conversion with a Metal−Organic Framework for Efficient and Selective Catalysis. *Angew. Chem., Int. Ed.* **2016**, *55* (11), 3685−3689.

(22) Stephenson, C. J.; Hupp, J. T.; Farha, O. K. Postassembly Transformation of a Catalytically Active Composite Material, Pt@ZIF-8, via Solvent-Assisted Linker Exchange. *Inorg. Chem.* **2016**, *55* (4), 1361−1363.

(23) Chizallet, C.; Lazare, S.; Bazer-Bachi, D.; Bonnier, F.; Lecocq, V.; Soyer, E.; Quoineaud, A.-A.; Bats, N. Catalysis of Trans-esterification by a Nonfunctionalized Metal-Organic Framework: Acido-Basicity at the External Surface of ZIF-8 Probed by FTIR and ab Initio Calculations. *J. Am. Chem. Soc.* **2010**, *132* (35), 12365−12377.

(24) Zhang, Q.; Lee, I.; Joo, J. B.; Zaera, F.; Yin, Y. Core−Shell Nanostructured Catalysts. *Acc. Chem. Res.* **2013**, *46* (8), 1816−1824.

(25) Park, K. S.; Ni, Z.; Côté, A. P.; Choi, J. Y.; Huang, R.; Uribe-Romo, F. J.; Chae, H. K.; O'Keeffe, M.; Yaghi, O. M. Exceptional Chemical and Thermal Stability of Zeolitic Imidazolate Frameworks. *Proc. Natl. Acad. Sci. U. S. A.* **2006**, *103* (27), 10186−10191.

(26) Koo, J.; Hwang, I.-C.; Yu, X.; Saha, S.; Kim, Y.; Kim, K. Hollowing out MOFs: Hierarchical Micro- and Mesoporous MOFs with Tailorable Porosity via Selective Acid Etching. *Chem. Sci.* **2017**, *8* (10), 6799−6803.

(27) Yonghwi, K.; Tao, Y.; Gyeongwon, Y.; Bagher, G. M.; Jaehyoung, K.; Eunsung, L.; June, C. S.; Kimoon, K. Hydrolytic Transformation of Microporous Metal-Organic Frameworks to Hierarchical Micro- and Mesoporous MOFs. *Angew. Chem., Int. Ed.* **2015**, *54* (45), 13273−13278.

(28) Shen, K.; Zhang, L.; Chen, X.; Liu, L.; Zhang, D.; Han, Y.; Chen, J.; Long, J.; Luque, R.; Li, Y.; Chen, B. Ordered Macro-Microporous Metal-Organic Framework Single Crystals. *Science* **2018**, *359* (6372), 206−210.

(29) Castelli, A.; de Graaf, J.; Marras, S.; Brescia, R.; Goldoni, L.; Manna, L.; Arciniegas, M. P. Understanding and Tailoring Ligand Interactions in the Self-Assembly of Branched Colloidal Nanocrystals into Planar Superlattices. *Nat. Commun.* **2018**, *9* (1), 1141.

(30) Huang, W.; Zhou, J.; Froeter, P. J.; Walsh, K.; Liu, S.; Kraman, M. D.; Li, M.; Michaels, J. A.; Sievers, D. J.; Gong, S.; Li, X. Three-Dimensional Radio-Frequency Transformers Based on a Self-Rolled-Up Membrane Platform. *Nat. Electron.* **2018**, *1* (5), 305−313.

(31) Yu, X.; Huang, W.; Li, M.; Comberiate, T. M.; Gong, S.; Schutt-Aine, J. E.; Li, X. Ultra-Small, High-Frequency, and Substrate-Immune Microtube Inductors Transformed from 2D to 3D. *Sci. Rep.* **2015**, *5*, 9661.

(32) Huang, W.; Yu, X.; Froeter, P.; Xu, R.; Ferreira, P.; Li, X. On-Chip Inductors with Self-Rolled-Up SiNx Nanomembrane Tubes: A Novel Design Platform for Extreme Miniaturization. *Nano Lett.* **2012**, *12* (12), 6283−6288.

(33) Song, Y.; Hu, D.; Liu, F.; Chen, S.; Wang, L. Fabrication of Fluorescent SiO2@Zeolitic Imidazolate Framework-8 Nanosensor for Cu2+ Detection. *Analyst* **2015**, *140* (2), 623−629.

(34) Guerra, R. E.; Kelleher, C. P.; Hollingsworth, A. D.; Chaikin, P. M. Freezing on a Sphere. *Nature* **2018**, *554*, 346.

(35) Pang, S. H.; Han, C.; Sholl, D. S.; Jones, C. W.; Lively, R. P. Facet-Specific Stability of ZIF-8 in the Presence of Acid Gases Dissolved in Aqueous Solutions. *Chem. Mater.* **2016**, *28* (19), 6960−6967.

(36) Michael, S. F.; Kilfoil, V. J.; Schmidt, M. H.; Amann, B. T.; Berg, J. M. Metal Binding and Folding Properties of a Minimalist Cys2His2 Zinc Finger Peptide. *Proc. Natl. Acad. Sci. U. S. A.* **1992**, *89* (11), 4796−4800.